# Nanotube Alignment Mechanism in Floating Evaporative Self-Assembly

*Katherine R. Jinkins[1], Jason Chan[2], Gerald J. Brady[1], Kjerstin K. Gronski[3], Padma Gopalan[1], Harold T. Evensen[4], Arganthaël Berson[2], Michael S. Arnold[1,*]*

[1]Department of Materials Science & Engineering, University of Wisconsin-Madison, 1509 University Ave., Madison, WI 53706

[2]Department of Mechanical Engineering, University of Wisconsin-Madison, 1513 University Ave., Madison, WI 53706

[3]Department of Chemistry, University of Wisconsin-Platteville, 1 University Plaza, Platteville, WI 53818

[4]Department of Engineering Physics, University of Wisconsin-Platteville, 1 University Plaza, Platteville, WI 53818

ABSTRACT

The challenge of assembling semiconducting single-wall carbon nanotubes (s-SWCNTs) into densely packed, aligned arrays has limited the scalability and practicality of high-performance nanotube-based electronics technologies. The aligned deposition of s-SWCNTs via Floating Evaporative Self-Assembly (FESA) has promise for overcoming this challenge; however, the mechanisms behind FESA need to be elucidated before the technique can be improved and scaled. Here, we gain a deeper understanding of the FESA process by studying a

stationary analog of FESA and optically tracking the dynamics of the organic ink/water/substrate and ink/air/substrate interfaces during the typical FESA process. We observe that the ink/water interface serves to collect and confine the s-SWCNTs before alignment and that the deposition of aligned bands of s-SWCNTs occurs at the ink/water/substrate contact line during a depinning of both the ink/air/substrate and ink/water/substrate contact lines. We also demonstrate improved control over the interband spacing, bandwidth, and packing density of FESA-aligned s-SWCNT arrays. The substrate lift rate (5 – 15 mm $min^{-1}$) is used to tailor the interband spacing from 90 to 280 μm while maintaining a constant aligned s-SWCNT bandwidth of 50 μm. Varying the s-SWCNT ink concentration (0.75 – 10 μg $mL^{-1}$) allows control of the bandwidth from 2.5 to 45 μm. A steep increase in packing density is observed from 11 s-SWCNTs $\mu m^{-1}$ at 0.75 μg $mL^{-1}$ to 20 s-SWCNTs $\mu m^{-1}$ at 2 μg $mL^{-1}$, with a saturated packing density of ~24 s-SWCNTs $\mu m^{-1}$. We also demonstrate scaling of FESA to align s-SWCNTs on a 2.5 × 2.5 $cm^2$ scale while preserving high quality alignment on the nanometer scale. These findings promise to help realize the scalable fabrication of well-aligned s-SWCNT arrays to serve as large-area platforms for next-generation semiconductor electronics.

## INTRODUCTION

Studies of individual semiconducting single-wall carbon nanotubes (s-SWCNTs) have shown that s-SWCNTs exhibit exceptional electronic properties including high charge carrier mobility and current carrying capacity, making them attractive candidates for next-generation field effect transistors (FETs) for thin film, radio frequency, and semiconductor electronics technologies.[1–4] These FETs will need to be fabricated from aligned arrays of multiple s-SWCNTs in order to maximize their performance – as opposed to single s-SWCNTs or networks

of randomly oriented s-SWCNTs. However, the scalable assembly of s-SWCNTs into densely packed, aligned arrays has been challenging.[5]

Several approaches have been researched for fabricating arrays or films of s-SWCNTs with increased alignment. These approaches include the direct growth of aligned arrays via chemical vapor deposition and deposition from solution.[6] However, direct growth typically results in the production of both metallic SWCNTs (m-SWCNTs) and s-SWCNTs, and the m-SWCNTs must be removed post-growth to ensure a high FET on/off ratio. Solution processing is often preferable as m-SWCNTs can be removed prior to deposition using conjugated polymer wrappers[7] or similar methods[8] to produce inks of highly purified s-SWCNTs. Solution processing can also be performed at room temperature on arbitrary surfaces, while direct growth via CVD is at high temperature, limiting the surfaces on which SWCNTs can be grown. s-SWCNTs in solution have been assembled onto substrates via Langmuir-Blodgett[9] and -Schaefer methods,[10,11] vacuum filtration,[12] blown-bubble assembly,[13] dielectrophoresis,[14] shear,[15] evaporative self-assembly,[16] and recently Floating Evaporative Self-Assembly (FESA)[17] – all which have progressed towards the ultimate goal of achieving highly aligned s-SWCNT arrays via a scalable process. FESA is of particular interest as it promises excellent scalability and yields aligned arrays from organic inks of s-SWCNTs near the intermediate packing density (~100 s-SWCNTs $\mu m^{-1}$) needed for achieving high FET conductance. For example, FETs fabricated from FESA-aligned s-SWCNTs have outperformed gallium arsenide (GaAs) and silicon (Si) FETs with respect to on-state current density and conductance.[18]

In FESA, a vertical substrate is lifted out of a water trough while s-SWCNTs in organic solvent (s-SWCNT ink) is sequentially dosed in μL droplets at the air/water/substrate contact

line.[17] The ink droplets spread rapidly on the water surface with each droplet resulting in the deposition of a band of aligned s-SWCNTs across the substrate.

FESA was initially termed "Floating Evaporative Self-Assembly" because it was believed the mechanism of FESA was similar to that of conventional evaporative self-assembly. However, as the results discussed below illustrate, the mechanisms controlling the deposition and alignment of s-SWCNTs in each process are distinct. In evaporative self-assembly, a single solvent evaporates, with the substrate being translated out of the solvent in some variants of the method. The evaporation induces the convective transport of nanostructures to the substrate-solvent-air contact line, resulting in the deposition of dense 'coffee rings' of ordered nanostructures such as s-SWCNTs.[19,20] However, unlike evaporative self-assembly, FESA utilizes two liquid phases (the organic solvent and the water subphase), and, practically, the time scale of FESA is much shorter than evaporative self-assembly (seconds and minutes compared to hours or even days). Moreover, even though there is evaporation of the organic solvent in FESA, it does not contribute to the alignment of the s-SWCNTs (as shown below), and the small fraction of the organic solvent that does evaporate is rapidly replenished via subsequent dosing of the ink.

More similar to FESA in method than evaporative self-assembly, the Langmuir-Blodgett and -Schaefer approaches for aligning nanostructures both employ two liquid phases. In the Langmuir-Blodgett and -Schaefer methods, a nanostructure-containing organic ink is spread on a water trough. After the solvent completely evaporates, barriers are used to closely pack nanostructures, such as s-SWCNTs, into well-ordered arrays.[9,10] However, there are three key differences between FESA and the Langmuir-Blodgett and -Schaefer methods: (i) during FESA, the organic solvent is never allowed to completely evaporate; (ii) during FESA, the organic

solvent is still spreading as the nanostructures deposit onto the substrate; and (iii) barriers are not needed during FESA to induce alignment in the films (as used in the Langmuir-Blodgett and -Schaefer methods).

An additional approach to assembling nanostructures is to use a two-phase system in which neither phase evaporates and nanostructures that assemble at the interface are transferred to substrates. Unlike Langmuir-Blodgett and –Schaefer methods, this approach does not require a barrier. Two-phase assembly has been employed previously to obtain aligned assemblies of nanowires and nanorods[21,22] and randomly aligned films of nanotubes and graphene.[23,24] Such studies suggest that the segregation of s-SWCNTs at the liquid/liquid interface may also be important during FESA; although one important difference between FESA and these previous two-phase assembly methods is that FESA is a dynamic process during which organic ink layer spreads and flows.

These significant distinctions between the FESA technique and other similar nanostructure alignment strategies motivate an in-depth study into the mechanisms underpinning FESA. A complete understanding of the FESA approach promises to guide future research in the control and manipulation of aligned arrays of s-SWCNTs. Here, we gain detailed insight into FESA by both studying a stationary analog of FESA (termed Stationary FESA) and optically tracking the ink/air/substrate and ink/water/substrate contact lines during the typical FESA process (termed Dose FESA) and then correlating the positions of these interfaces with the positions of the deposited s-SWCNTs. We learn that, first, the ink/water interface serves to collect and confine s-SWCNTs during FESA. Second, s-SWCNTs deposit onto the substrate from the ink/water interface during the depinning of the ink/water/substrate and ink/air/substrate interfaces. The depinning of the interfaces and the outward spreading of ink likely aid in the

alignment of the already-confined s-SWCNTs as they deposit onto the substrate. We also show that the substrate lift rate can be used to dictate the spacing between the bands of aligned s-SWCNTs and that the ink concentration controls both bandwidth and packing density. Finally, we demonstrate the scaling of FESA to a 2.5 cm by 2.5 $cm^2$ deposition area.

## EXPERIMENTAL SECTION

### Preparation of PFO-BPy Wrapped s-SWCNTs

s-SWCNTs are isolated using a 1:1 ratio by weight of arc-discharge CNT soot (698695, Sigma-Aldrich) and a polyfluorene derivative, poly[(9,9-dioctylfluorenyl-2,7-diyl)-alt-co-(6,6′-{2,2′-bipyridine})] (PFO-BPy), (American Dye Source, Inc., Quebec, Canada; #ADS153-UV), which are each dispersed at a concentration of 2 mg $mL^{-1}$ in toluene. 60 mL of this mixture is sonicated with a horn tip sonicator (Fisher Scientific, Waltham, MA; Sonic dismembrator 500) for 30 min. The solution is centrifuged in a swing bucket rotor at $3 \times 10^5$ *g* for 10 min to remove undispersed material. The top 90% of the supernatant is collected, centrifuged for 18-24 h, and dispersed in toluene with sonication via the horn tip sonicator. This latter process is repeated three times to rinse off as much excess PFO-BPy as possible. The final solution is prepared by horn-tip sonication of the rinsed s-SWCNT pellet in chloroform (stabilized with ethanol from Fisher Scientific, #C606SK-1). The concentration of the s-SWCNTs is determined using optical cross sections from the $S_{22}$ transition.[7]

### Preparation of Substrates for FESA Processes

$Si/SiO_2$ and quartz substrates are employed. The substrates are cleaned with a piranha solution of 2:1 ratio by volume of $H_2SO_4$ (91 – 92.5%):$H_2O_2$ (30%) in a 340 mL crystallizing dish on a hotplate set to 110 °C for 60 min, rinsed with deionized water, and dried with $N_2$. After

piranha treatment, the substrates are exposed to hexamethyldisilizane (HMDS) vapor (Solitec VBS200 HMDS Prime Oven) for 10 s to create a hydrophobic self-assembling monolayer (vapor deposition). Prior to HMDS deposition, the substrates are baked in an ambient environment on a hotplate set to 205 °C for 325 s to drive off water from the substrate surface. The water contact-angle on the HMDS treated substrates is ~45°.

**Back-Imaging of Contact Line Dynamics**

Transparent quartz substrates are used to enable optical imaging of the FESA process in transmission. As shown in Fig. S1, the back of each quartz substrate is coated with polytetrafluoroethylene (PTFE) to subdue the water contact line on the back of the substrate. This allows clear imaging of the buried ink/water interface through the substrate during deposition. The PTFE films are fabricated from 2% by mass PTFE (Sigma-Aldrich 469629) in perfluorodecalin 95% (Sigma-Aldrich P9900). This solution is spun-cast on the quartz substrates at 2500 rpm. The films are then baked in $N_2$ on a 200 °C hot plate for 1 h. Images are recorded at 100 frames per second (fps) using a Basler acA2000-165uc camera mounted with a Navitar 12*x* objective lens. The images are backlit using a Fiber-Lite PL-800 light mounted with fiber optics.

**MATLAB Processing on Images**

Tracking of the contact lines is performed using MATLAB. First, original red, green, blue (RGB)-colored images are converted to grayscale-level arrays, and contrast and brightness are adjusted to emphasize the interfaces. A median filter is subsequently applied to smooth out pixel noise. The exposure time and lighting are constant during the experiment so the same adjustments (contrast, brightness, and filter) are applied to every image in the set. After converting to grayscale, the ink/air/substrate contact line is located by finding the local

maximum of the gradient of grayscale values in each column of pixels. The contrast at the ink-water-substrate contact line is much weaker and requires a different approach. First, the area of interest is limited to the region below the previously detected ink-air-substrate contact line. The reduced image is binarized using Otsu's algorithm (*imbinarize* function in MATLAB) in order to show the ink film as bright pixels (see Fig. S2). Spurious bright pixels are filtered out using an in-house algorithm. The ink/water/substrate contact line is determined as the bottom boundary of the bright region corresponding to the ink film. Both detected contact lines are finally smoothed using a moving average.

**Deposition Parameters for Figures**

Figure 1. The ink concentration is 10 μg $mL^{-1}$. 15 μL of water and 10 μL of ink are used. Figure 2. The ink concentration is 10 μg $mL^{-1}$. The ink doses are 1 μL. The needle/substrate distance is 1.27 mm. The dose frequency is 50 $min^{-1}$. The substrate lift rate is 7 mm $min^{-1}$. Figure 3. The ink concentration is 10 μg $mL^{-1}$. The ink doses are 1 μL. The needle/substrate distance is 1.27 mm. The dose frequency is 50 $min^{-1}$. The substrate lift rate is 7 mm $min^{-1}$. Figure 4. The ink doses are 1 μL. The needle/substrate distance is 1.27 mm. The dose frequency is 50 $min^{-1}$. The substrate lift rate is 7 mm $min^{-1}$. Figure 5. The ink concentration is 10 μg $mL^{-1}$. The ink doses are 2.5 μL. The dose frequency is 50 $min^{-1}$. The substrate lift rate is 9 mm $min^{-1}$. The needle/substrate distance is 3.8 mm. A larger needle/substrate distance is used compared to the depositions in Figs. 2, 3 and 4 because the ink volume is larger and more time (i.e. distance for the ink to travel before hitting the substrate) is needed to form a uniform ink front.

RESULTS AND DISCUSSION

**Stationary FESA**

We first study a simplified table-top version of the FESA method, Stationary FESA. A water trough is not used; instead, a small 15 μL water droplet is placed on a stationary, horizontal substrate. A single 10 μL dose of ink is deposited on top of the water droplet, yielding a single aligned band of s-SWCNTs at the ink/water/substrate contact line. Stationary FESA provides a simple way to measure the position of ink/water contact line on the substrate and compare it with the position of the resulting deposited s-SWCNTs.

When the s-SWCNT ink is delivered during Stationary FESA, the ink spreads quickly around the water droplet, creates a 'skirt' at the base of the droplet (Fig. 1a), and then evaporates. The air/water/substrate contact line moves inwards during this process yielding a more hydrophobic contact angle (Fig. 1b). After the solvent has evaporated, the water droplet is manually removed using a syringe and scanning electron microscopy (SEM) (Zeiss Leo 1530) is used to characterize the s-SWCNTs deposited on the substrate. The s-SWCNTs that deposit at the ink/air/substrate contact line are randomly oriented (Fig. 1c). Dense stripes of randomly oriented s-SWCNTs are observed and are attributed to a 'coffee-stain' effect caused by the dynamical pinning and zipping motion of the ink/air/substrate interface as the solvent evaporates.[19] In constrast, the s-SWCNTs that deposit at the ink/water/substrate contact line are well aligned, similar to the alignment previously demonstrated by Dose FESA[17,18] (Fig. 1d). The aligned s-SWCNTs that deposit at the edge of the water droplet are responsible for pinning the droplet at the more hydrophobic contact angle previously noted.

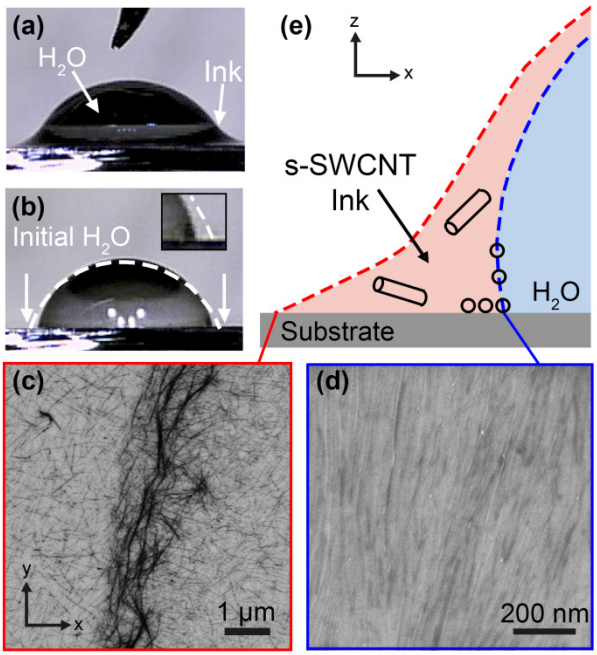


**Figure 1**. Stationary FESA experiments elucidate deposition and alignment mechanisms. (a-b) Optical images during and after the Stationary FESA process. (a) A droplet of s-SWCNT ink is applied to a stationary water droplet on a $SiO_2$/Si substrate. The ink spreads uniformly around the water droplet forming a 'skirt' around the base. (b) The ink evaporates in ~5 s, creating deposits of s-SWCNTs which pin the final water contact line. The initial outline of the water droplet is indicated in white. Inset shows zoomed-in view of the right side of the droplet. (c) SEM image of coffee-stain deposition occurring at the ink/air interface. (d) SEM micrograph of aligned s-SWCNT deposition occurring at ink/water interface. (e) Schematic of the stationary deposition event indicating that aligned SWCNT deposition occurs at the ink/water/substrate contact line. Coordinate systems are shown in (c) and (e) to clarify the orientation of the deposited s-SWCNTs with respect to the droplet geometry. The coordinates in (c) also apply to (d).

The results of these Stationary FESA experiments are surprising and indicate that the aligned deposition of s-SWCNTs occurs at the ink/water/substrate contact line (Fig. 1d). In contrast, related studies have shown that surfactant encapsulated s-SWCNTs dispersed in aqueous solution align and deposit at the air/water/substrate contact line as the water evaporates. One potential explanation for the deposition of s-SWCNTs at the ink/water/substrate contact line during Stationary FESA is that s-SWCNTs accumulate at this ink/water interface. Related studies have shown that nanostructures, such as graphene nanosheets, collect and assemble at organic solvent/water interfaces.[23] To examine if polyfluorene-wrapped s-SWCNTs would similarly assemble at the chloroform/water interface, we create an emulsion of s-SWCNT chloroform ink in water and let it settle (Fig. S3). The s-SWCNTs are seen to collect at the chloroform/water interface (Fig. S3b). This observation, in conjunction with results from Stationary FESA experiments, indicates that the collection and confinement of s-SWCNTs at the ink/water interface are important aspects of the FESA process.

**s-SWCNT Assembly using Dose FESA**

The Dose FESA process is more complex than Stationary FESA due to the periodic dosing of ink droplets at the aqueous subphase, the spreading of these droplets, and the translation of the substrate. In order to determine if the collection and confinement of s-SWCNTs at the ink/water interface also plays an important role in Dose FESA, a separate experimental apparatus (Fig. S1) is constructed that enables optical imaging of the dynamics of the ink/air/substrate and ink/water/substrate contact lines through a transparent quartz substrate. A 100 fps camera (Basler acA2000-165uc) is used to record the motion of the contact lines as a series of images. The recorded images are analyzed to track the separate positions of the contact lines.

In these experiments, doses of s-SWCNT-containing organic ink are delivered to an aqueous subphase via a needle that is in direct contact with the surface of the subphase. The contact of the needle tip with the surface provides a more reproducible means for controlling the timing and volume of ink delivery compared with our previous work in which a needle was suspended above the surface releasing drops more sporadically.[17] A syringe pump (Chemyx Nexus 3000) is used to precisely control the volume of each dose of ink and the frequency of the doses. Each dose of ink yields an ordered band of deposited s-SWCNTs that are aligned within a ±10° window, as determined by polarized Raman spectroscopy (see discussion in Supporting Information and Fig. S4), consistent with our previous FESA studies.[17]

Traces of the contact lines are shown in Fig. 2a for an experiment in which 1 μL doses of ink are pulsed every 1.2 s. The traces are analyzed in the reference frame of the substrate by subtracting the substrate lift rate (7 mm $min^{-1}$). The traces indicate that immediately after ink is pulsed (denoted by green arrows), both the ink/air/substrate and ink/water/substrate contact lines quickly drop. These events are denoted by the symbols (&) and (%) for ink/air/substrate and ink/water/substrate contact lines, respectively. The distance between the ink/air/substrate and ink/water/substrate contact lines is ~250 μm and is invariant over the course of the experiment. This distance corresponds to the thickness of the chloroform ink layer near the substrate. For comparison, the evaporation rate is only 20.4 μm per 1.2 s (calculation in Supporting Information and Fig. S5).

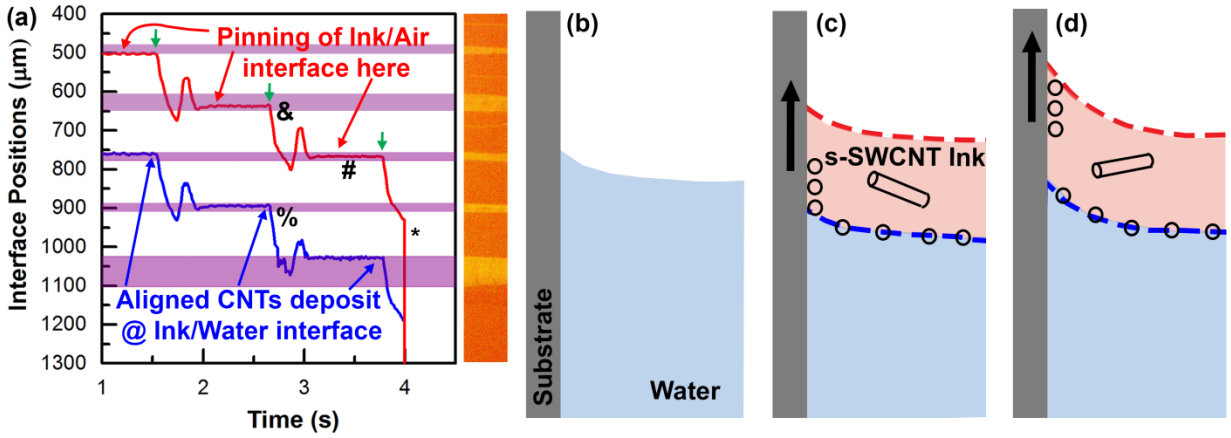


**Figure 2.** Dynamics of Dose FESA. (a) Traces of ink/water/substrate and ink/air/substrate contact lines as a function of time, in the frame of reference of the substrate. Cross-polarized optical microscopy image of aligned s-SWCNT bands spatially registered with the traces. The symbols (&) and (%) denote the fall of the ink/air/substrate and ink/water/substrate contact lines, respectively. (#) denotes pinning of the ink/air/substrate contact line and (*) indicates where the substrate is lifted out of the water at a high lift rate to prevent the ink/air/substrate interface from pinning and drying on the last band deposited. The green arrows indicate when new doses of ink are added. Small oscillations in the positions of the contact lines occur directly after each dose. These oscillations may be indicative of small oscillations in the volumetric flow rate of ink as the ink exits the needle and/or the reflection of surface waves off of the substrate or needle or a combination of the two. Panels (b-d) depict important aspects of FESA. (b) Initially, the substrate is partially submerged in a trough of water. (c) s-SWCNT ink is delivered at the air/water interface. The ink/water interface (dashed blue line) and the ink/air interface (dashed red line) form. A fraction of the s-SWCNTs accumulate at the ink/water interface (dashed blue line) and deposit onto the substrate from this interface. (d) As the substrate is lifted out of the water, the ink/air/substrate contact line is pinned on a previously-deposited band of aligned s-SWCNTs

until the next dose of ink is delivered. Variations in band spacing and width are due to insufficient vibration control for this particular experiment.

Using registration marks, we are able to register the positions of the contact lines to the positions of the aligned bands of s-SWCNTs deposited on the substrate (see Figs. S2, S6, S7 for more details regarding the registration protocol). A registered cross-polarized optical image of aligned s-SWCNTs is shown on the right side of Fig. 2a. Comparing this image to the traces, it is apparent that the bands of aligned s-SWCNTs deposit onto the substrate shortly after each pulse is delivered, just as the contact lines begin to drop. The dropping of the contact lines and the spreading of the newly delivered ink droplets must both contribute to tangential flows directed parallel to the contact lines. We hypothesize that these flows aid in aligning the s-SWCNTs as they deposit onto the substrate from the ink/water interface. Both of the contact lines fall until the ink/air/substrate contact line is pinned by the previously deposited band of aligned s-SWCNTs, as denoted in Fig. 2a by the symbol (#). The pinning of the ink/air/substrate contact line also fixes the ink/water/substrate contact line.

The pinning of the ink/air/substrate contact line on previously deposited bands of aligned s-SWCNTs raises a question. How can we be sure that aligned bands of s-SWCNTs are not formed by the evaporation of ink and the deposition of s-SWCNTs at the ink/air/substrate contact line since this contact line is repeatedly coincident with the aligned bands, as denoted by the symbol (#)? To answer this question, at the end of the experiment tracked in Fig. 2a, the substrate is rapidly withdrawn from the aqueous subphase at a rate of 50 mm $min^{-1}$, as denoted by symbol (*). This rapid withdrawal prevents the pinning of the ink/air/substrate contact line on the final band of s-SWCNTs. The existence of this final band therefore additionally confirms that

each band of aligned-SWCNTs is deposited not from the ink/air/substrate but rather the ink/water/substrate contact line.

These processes are summarized schematically in Figs. 2b-d. Fig. 2b depicts the substrate and water prior to starting the FESA deposition. When the ink is pulsed, nearly simultaneously the s-SWCNTs become confined at the ink/water interface, the ink droplet spreads, and the water level falls near the substrate. The deposition of aligned SWCNTs occurs from the ink/water/substrate contact line at the beginning of this fall, potentially aided by tangential flows (Fig. 2c). As the substrate is raised, the ink/air/substrate contact line becomes pinned by previously deposited s-SWCNTs (Fig. 2d). Both air and water contact lines are raised along with the substrate until the next pulse of ink arrives and unpins the contact lines.

None of these aspects require the evaporation of the organic solvent from the ink. To confirm that the evaporation of the solvent is not a critical factor during FESA, we next conduct an experiment in which the air is nearly saturated with chloroform vapor to suppress evaporation of the ink as the ink spreads and the s-SWCNTs deposit. Similar s-SWCNT deposition and alignment are observed (Fig. S8). Moreover, to further explore if flow and spreading of the organic ink are important parameters during FESA, we conduct an additional experiment without flow (and without evaporation) by layering a relatively thick, uniform, and stagnant layer of s-SWCNT ink on top of the aqueous subphase and withdrawing the substrate through the solvent/water interface. The s-SWCNTs that deposit onto the substrate are randomly aligned in some regions and partially aligned in other regions but without a direction of global alignment (Fig. S9). These results further indicate that the accumulation of s-SWCNTs at the solvent/water interface is by itself insufficient to drive the broad alignment of s-SWCNTs without the aid of tangential flows.

In addition to tangential flows, liquid crystal-like interactions and SWCNT-SWCNT crowding effects may also contribute to the ordering of s-SWCNTs at the liquid/liquid interface. However, the fact that excellent alignment of s-SWCNTs is observed even when the concentration of the ink and the resulting packing density of s-SWCNTs are dramatically decreased (as shown, below, Fig. 4a) suggest that liquid crystal-like interactions and SWCNT-SWCNT crowding effects are not the primary factors leading to alignment.

Another factor that likely affects the FESA process is the substrate surface energy. The substrate surface energy will affect the adhesion of CNTs to the substrate while at the same time dictating the contact angles and consequently the contact-line dynamics that follow each dose of ink. We expect that the necessary contact line dynamics and s-SWCNT adhesion will occur only for a certain range of substrate surface energies; and, therefore, detailed studies of substrate surface energy dependencies should be the focus of future investigations.

The knowledge gained that (i) the collection and confinement of s-SWCNTs at the ink/water interface and (ii) pinning and depinning dynamics are important factors during FESA guide the studies in the next section of this paper, which analyzes s-SWCNT ink concentration and substrate lift rate dependencies.

**Effect of Substrate Lift Rate and s-SWCNT Ink Concentration on FESA**

Accurate control over the positioning and bandwidth of FESA-deposited bands of aligned s-SWCNTs and excellent band-to-band uniformity are needed for commercialization efforts. To improve the regularity of the bands and their uniformity, the FESA apparatus is placed on a vibration isolation table and enclosed inside of an acrylic box to limit air drafts and acoustic vibrations from the laboratory environment. Without these steps, vibrations of the trough surface

cause band-to-band variation in both spacing and bandwidth (Fig. 2a). After implementing these measures, these variations are dramatically reduced thereby improving regularity and uniformity (Figs. 3, 4, 5, S7, and S10).

A variable that can be used to control FESA arrays is the substrate lift rate. As shown in Fig. 3a, the lift rate controls the spacing between bands of aligned s-SWCNTs without affecting bandwidth. SEM micrographs of substrates created using lift rates of 5, 11, and 15 mm $min^{-1}$ are shown in Fig. 3b, which result in an interband spacing measured at the center of each band of 91 ± 4, 170 ± 7, and 283 ± 7 µm, respectively, and bandwidth of 50 ± 2, 53 ± 3, and 53 ± 3 µm, respectively. The back-imaged contact line dynamics at 5 and 15 mm $min^{-1}$ lift rates (Fig. S10) show the same pinning/depinning behavior as seen in Fig. 2a.

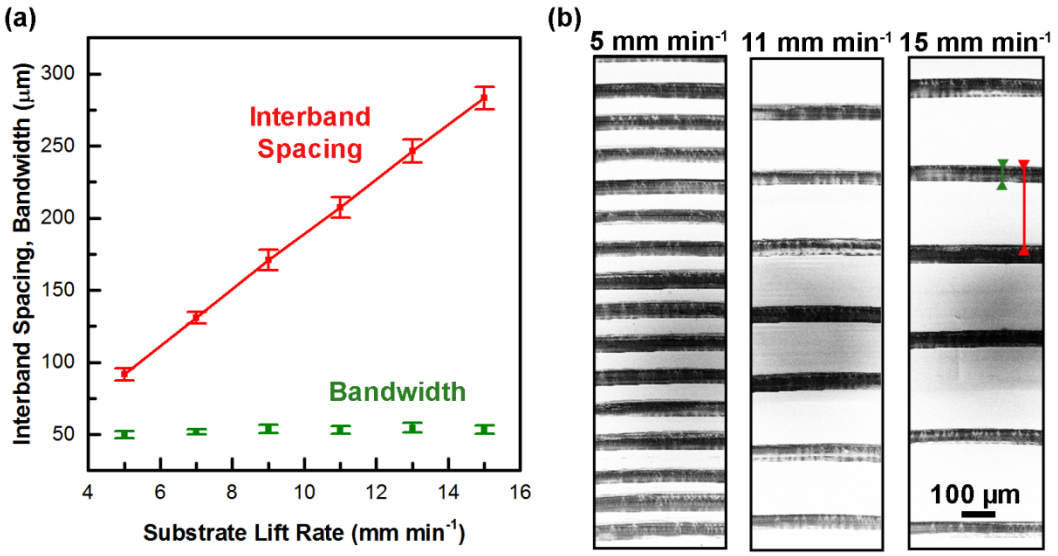


**Figure 3**. Dose FESA is a controllable process for s-SWCNT alignment. (a) Interband spacing and bandwidth as a function of substrate lift rate. Bandwidth is invariant while interband spacing increases linearly with lift-rate. (b) SEM micrographs of substrates prepared using lift rates of 5, 11, and 15 mm $min^{-1}$. The aligned bands are black in these micrographs.

The packing density of the FESA aligned s-SWCNT films can be controlled by varying the s-SWCNT ink concentration, at fixed dose volume. We find that an increase in ink concentration from 0.75 to 2 μg $mL^{-1}$ causes an increase in s-SWCNT packing density within each band from 11 to 20 s-SWCNTs $\mu m^{-1}$, as measured by SEM in Fig. 4a. However, with further increases in ink concentration, we observe a nonlinear relationship between concentration and packing density with the packing density increasing only to ~24 s-SWCNTs $\mu m^{-1}$. SEM micrographs of s-SWCNT films deposited using 0.75 and 7 μg $mL^{-1}$ are compared in Fig. 4b. It is not clear from SEM or AFM measurements (Fig. S11) if some of the s-SWCNTs counted for packing density measurements are fibers of multiple parallel tubes. However, the measured height of the s-SWCNT films does not change in the saturated regime, indicating that the total number of s-SWCNTs deposited in this regime is indeed invariant with s-SWCNT ink concentration. We hypothesize that the initial increase in packing density with increasing ink concentration can be attributed to a concomitant increase in the concentration of s-SWCNTs confined at the ink/water interface. To explain the packing density saturation, our hypothesis is that the concentration of s-SWCNTs at the ink/water interface saturates. Once saturated, further increases in the bulk concentration of the ink do not affect the concentration of s-SWCNTs at the interface, which, in turn, do not affect the packing density of the s-SWCNTs deposited within the bands.

The density of s-SWCNTs that deposit onto the substrate will not only be governed by the density of the s-SWCNTs at the ink/water interface but also by the energetics of their adsorption to the substrate, the spreading of the ink droplet, and the contact line dynamics. These factors will be affected by the surface treatment of substrate, the substrate-needle geometry, and mode of ink delivery. While the surface treatment, the substrate-needle geometry, and ink delivery are all held constant in this study, yielding a saturated packing density of 24 s-SWCNTs $\mu m^{-1}$, other configurations may yield different saturated packing densities. For example, a packing density of 50 s-SWCNTs $\mu m^{-1}$ has been observed when delivering ink via gravity-released droplets.[17]

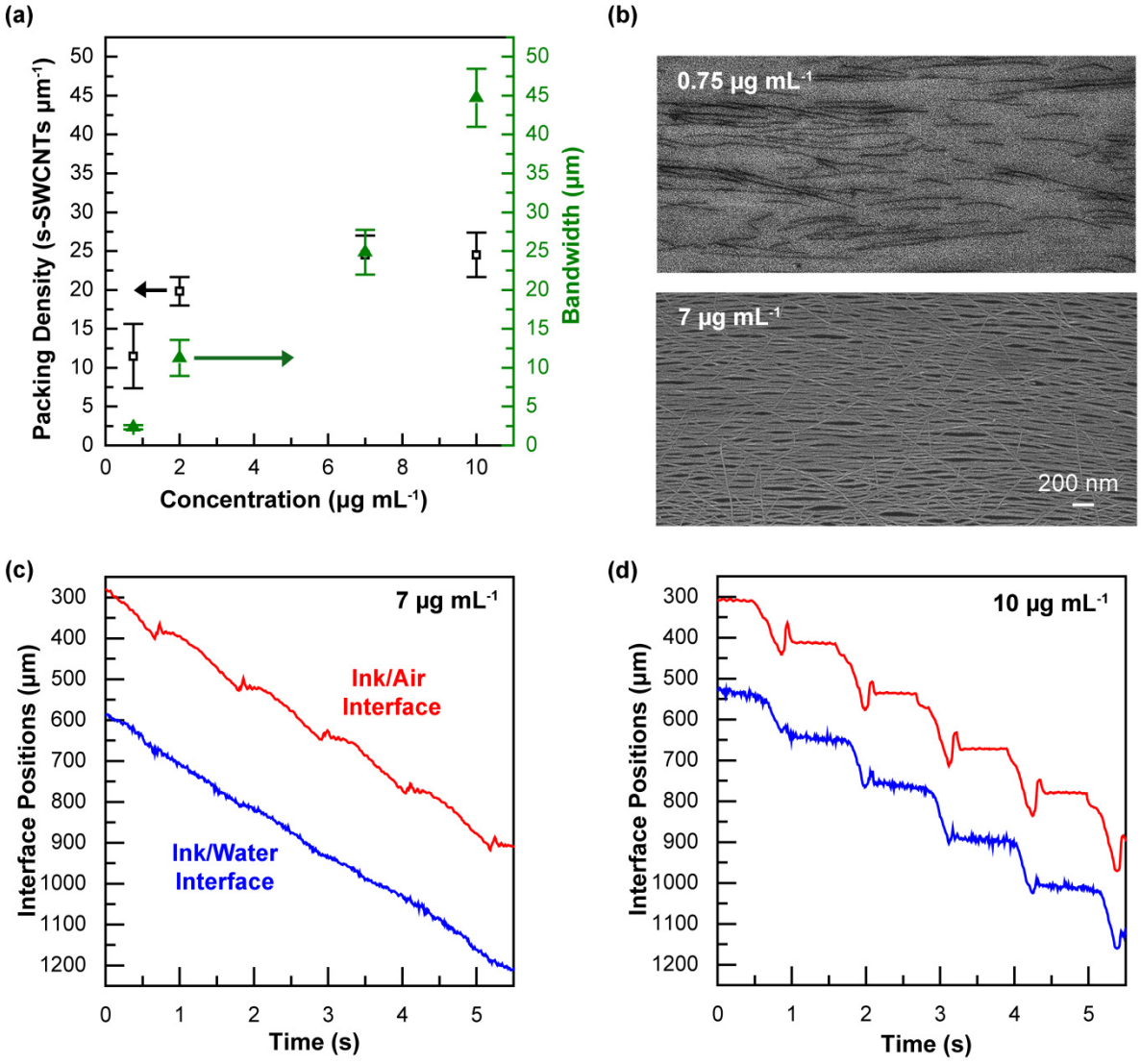

**Figure 4**. (a) Bandwidth and packing density of deposited aligned s-SWCNTs increase with increasing concentration. Packing density initially increases and then quickly saturates at ~24 s-SWCNTs $\mu m^{-1}$. (b) SEM micrographs showing packing density and alignment at 0.75 and 7 $\mu g\ mL^{-1}$. (c-d) Traces of ink/air/substrate and ink/water/substrate contact lines in the frame of the substrate from concentrations (c) 0.25 $\mu g\ mL^{-1}$ and (d) 10 $\mu g\ mL^{-1}$. Larger concentrations show more pinning/depinning of the contact lines. In this figure, the substrate lift rate is held constant across experiments at 7 mm $min^{-1}$.

The bandwidth is also affected by the concentration of s-SWCNTs in the ink. Figs. 4c-d are back-imaging traces of the contact lines for s-SWCNT depositions using ink concentrations of 0.25 and 10 $\mu g\ mL^{-1}$, respectively. At 0.25 $\mu g\ mL^{-1}$, there is relatively minimal pinning and depinning behavior yielding a narrow bandwidth. Determining the smallest bandwidth that can be achieved with this method is difficult because the packing density also simultaneously decreases as the s-SWCNT concentration is decreased, eventually yielding ill-defined bands (Fig. 4b). At higher s-SWCNT concentrations, there is more pinning, lasting for longer duration, yielding a larger deposited bandwidth upon depinning.

**Aligned s-SWCNT Arrays over 2.5 x 2.5 $cm^2$ via Dose FESA**

We demonstrate that FESA can be used to deposit well-aligned s-SWCNTs over large areas of 2.5 × 2.5 $cm^2$ by optimizing the deposition parameters. For this demonstration, 1.5 µL doses of ink at a s-SWCNT concentration of 10 $\mu g\ mL^{-1}$ are pulsed at a frequency of 50 $min^{-1}$ with a substrate lift rate of 9 mm $min^{-1}$. As a result, it takes less than 3 min to deposit aligned bands of s-SWCNTs across the entire substrate. An optical image of the resulting sample is

shown in Fig. 5a. In this image, obtained using a conventional digital camera (Nikon D3100), the aligned bands of s-SWCNTs are visible and appear purple (Figs. 5a and 5b).

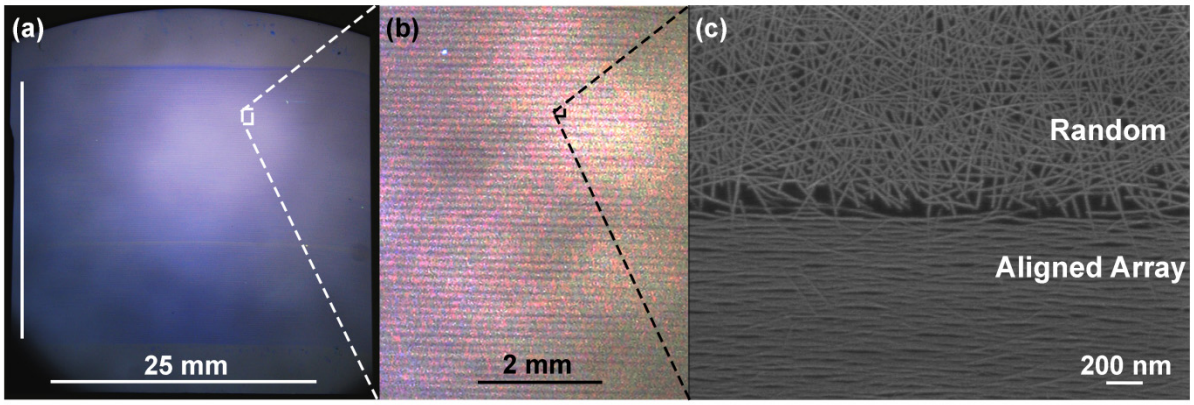


**Figure 5.** Dose FESA is a scalable process for creating aligned arrays of s-SWCNTs. (a-c) Dose FESA substrate of aligned s-SWCNTs on a centimeter, millimeter, and nanometer scale, respectively. (a) and (b) are optical photographs. In (a), the aligned s-SWCNT bands appear blue. In (b) the aligned bands are dark. (c) shows an SEM image of dense, well-aligned s-SWCNTs at the top of a band.

The SEM image in Fig. 5c characterizing the top of an aligned s-SWCNT band shows that the areas between bands of aligned s-SWCNTs contain randomly oriented s-SWCNTs. It is not yet clear whether the random s-SWCNTs deposit from the evaporating ink/air/substrate contact line, from the bulk of the ink solution, or from the ink/water/substrate after the bands of aligned s-SWCNTs are deposited. However, these randomly oriented s-SWCNTs can be removed using conventional lithography procedures as a result of the highly regular band spacing. We also observe the bandwidth narrowing from the center of the substrate 122 ± 13 μm to 25 ± 6 μm near the edge of the substrate. Future work will focus on improving the uniformity

of the aligned s-SWCNTs across the width of the substrate. This demonstration shows that the build-up of s-SWCNTs at the ink/water interface, the pinning and depinning of the contact lines, and the deposition of aligned bands of s-SWCNTs can be iteratively repeated many times without loss of fidelity, enabling large-area scaling.

## CONCLUSIONS

In this work, we show that FESA can be scaled to deposit s-SWCNTs over areas of 2.5 × 2.5 $cm^2$ while also retaining a high degree of nanoscale alignment, signifying an important step towards wafer-scale alignment of s-SWCNTs. We also investigate the mechanism of the controlled alignment of s-SWCNTs via FESA. While evaporation is part of the FESA acronym, we show that evaporation is not essential to the alignment of s-SWCNTs in this technique. The alignment occurs at the buried ink/water interface where evaporation is not expected to have a significant effect. Therefore, the mechanism that drives s-SWCNT alignment during FESA is entirely distinct from previously reported evaporative self-assembly methods.[19] During FESA, the deposition of the aligned s-SWCNTs occurs at the ink/water/substrate contact line as this contact line falls and sweeps across the substrate after the depinning of the ink/water/substrate and ink/air/substrate contact lines following the delivery of a dose of ink. We also find that the concentration of the s-SWCNT ink can be used to control the bandwidth and packing density of the aligned s-SWCNTs. Our data additionally show that s-SWCNTs collect and confine at the ink/water interface and that a small change in s-SWCNT concentration results in a large change in packing density until the packing density saturates. The insight regarding FESA mechanisms provided here may create new opportunities for scaling and improving s-SWCNT alignment and in particular implementing FESA to realize continuous rather than banded aligned arrays of s-SWCNTs. New opportunities may also arise for exploiting confinement at liquid-liquid

interfaces and the FESA process to align and deposit other types of anisotropic nanostructures beyond s-SWCNTs.

ASSOCIATED CONTENT

**Supporting Information**

The Supporting Information is available free of charge on the ACS Publications website at DOI: XXX.

Back-imaging setup; example image from back-imaging; optical images of water layered on s-SWCNT ink before and after mixing; discussion of measurement and polarized Raman spectra and SEM of 10 μg $mL^{-1}$ FESA sample; discussion of and calculation of chloroform evaporation rate; example of contact line tracking; example traces of ink/water/substrate and ink/air/substrate contact lines and their registration; SEM from chloroform vapor saturated FESA; setup and SEM from experiments withdrawing a substrate through a thick stagnant s-SWCNT ink layer; back-imaging traces at different substrate lift rates; and AFM images/height profiles of FESA aligned s-SWCNT films (PDF).

AUTHOR INFORMATION

**Corresponding Author**

*E-mail: michael.arnold@wisc.edu.

**Author Contributions**

K.R.J fabricated samples and performed the experiments and data processing for the Dose FESA experiments. J.C. and A.B. developed the MATLAB analysis code for tracking the contact lines.

G.J.B., K.K.G., and H.T.E. performed preliminary back-imaging experiments. G.J.B. and H.T.E. performed the Stationary FESA and the deposition from a thick, stagnant layer of s-SWCNT ink experiments. M.S.A. and A.B. supervised the work. All authors contributed to data interpretation. K.R.J. drafted the manuscript, and all authors discussed and revised it.

**Notes**

The authors declare no competing financial interest.

ACKNOWLEDGMENT

This work was primarily supported by the NSF-CMMI award No. 1462771 (K.R.J., G.J.B., M.S.A.). Partial support is also acknowledged from a supplement to NSF-CMMI award No. 1129802 to support researchers from a primarily undergraduate institution (K.K.G, H.T.E.). Partial support is also acknowledged from a seed grant from the Research and Innovation Committee at the University of Wisconsin-Madison (J.C., A.B.). K.R.J. and G.J.B. furthermore acknowledge support from the NSF Graduate Research Fellowship Program, award No. DGE-1256259. The authors gratefully acknowledge use of facilities and instrumentation supported by NSF through the University of Wisconsin Materials Research Science and Engineering Center (DMR-1121288, 0079983, and 0520057) and through the University of Wisconsin Nanoscale Science and Engineering Center (DMR-0832760 and 0425880).

**References**

(1) Dürkop, T.; Getty, S. A.; Cobas, E.; Fuhrer, M. S. Extraordinary Mobility in Semiconducting Carbon Nanotubes. *Nano Lett.* **2005**, *4*, 35–39.

(2) Avouris, P.; Appenzeller, J.; Martel, R.; Wind, S. J. Carbon nanotube electronics. *Proc. IEEE* **2003**, *9*, 1772–1784.

(3) Javey, A.; Guo, J.; Wang, Q.; Lundstrom, M.; Dai, H. Ballistic Carbon Nanotube Field-Effect Transistors. *Nature* **2003**, *424*, 654–657.

(4) Cao, Q.; Tersoff, J.; Farmer, D. B.; Zhu, Y.; Han, S. J. Carbon nanotube transistors scaled to a 40-nanometer footprint. *Science* **2017**, *356*, 1369–1372.

(5) Iakoubovskii, K. Techniques of aligning carbon nanotubes. *Cent. Eur. J. Phys.* **2009**, *7*, 645-653.

(6) Cantoro, M.; Hofmann, S.; Pisana, S.; Scardaci, V.; Parvez, A.; Ducati, C.; Ferrari, A. C.; Blackburn, A. M.; Wang, K. Y.; Robertson, J. Catalytic Chemical Vapor Deposition of Single-Wall Carbon Nanotubes at Low Temperatures. *Nano Lett.* **2006**, *6*, 1107–1112.

(7) Nish, A.; Hwang, J.-Y.; Doig, J.; Nicholas, R. J. Highly selective dispersion of single-walled carbon nanotubes using aromatic polymers. *Nat. Nanotechnol.* **2007**, *2*, 640–646.

(8) Hersam, M. C. Progress towards monodisperse single-walled carbon nanotubes. *Nat. Nanotechnol.* **2008**, *3*, 387–394.

(9) Li, X.; Zhang, L.; Wang, X.; Shimoyama, I.; Sun, X.; Seo, W. S.; Dai, H. Langmuir−Blodgett Assembly of Densely Aligned Single-Walled Carbon Nanotubes from Bulk Materials. *J. Am. Chem. Soc.* **2007**, *129*, 4890–4891.

(10) Cao, Q.; Han, S.-J.; Tulevski, G. S.; Zhu, Y.; Lu, D. D.; Haensch, W. Arrays of single-walled carbon nanotubes with full surface coverage for high-performance electronics. *Nat. Nanotechnol.* **2013**, *8*, 180–186.

(11) Sgobba, V.; Giancane, G.; Cannoletta, D.; Operamolla, A.; Omar, O. H.; Farinola, G. M.; Guldi, D. M.; Valli, L. Langmuir–Schaefer Films for Aligned Carbon Nanotubes Functionalized with a Conjugate Polymer and Photoelectrochemical Response Enhancement. *ACS Appl. Mater. Interfaces* **2014**, *6*, 153–158.

(12) He, X.; Gao, W.; Xie, L,; Li, B.; Zhang, Q.; Lei, S.; Robinson, J. M.; Hároz, E. H.; Doorn, S. K.; Wang, W.; Vajtai, R.; Ajayan, P. M.; Adams, W.W.; Hauge, R. H.; Kono, J. Wafer-scale monodomain films of spontaneously aligned single-walled carbon nanotubes. *Nat. Nanotechnol.* **2016**, *11*, 633–638.

(13) Yu, G.; Cao, A.; Lieber, C. M. Large-area blown bubble films of aligned nanowires and carbon nanotubes. *Nat. Nanotechnol.* **2007**, *2*, 372–377.

(14) Vijayaraghavan, A; Blatt, S; Weissenberger, D; Oron-Carl, M.; Hennrich, F.; Gerthsen, D.; Hahn, H.; Krupke, R. Ultra-Large-Scale Directed Assembly of Single-Walled Carbon Nanotube Devices. *Nano Lett.* **2007**, *7*, 1556–1560.

(15) Park, S.; Pitner, G.; Giri, G.; Koo, J. H.; Park, J.; Kim, K.; Wang, H.; Sinclair, R.; Wong, H. S. P.; Bao, Z. Large-Area Assembly of Densely Aligned Single-Walled Carbon Nanotubes Using Solution Shearing and Their Application to Field-Effect Transistors. *Adv. Mater.* **2015**, 27, 2656–2662.

(16) Engel, M.; Small, J. P.; Steiner, M.; Freitag, M.; Green, A. A.; Hersam, M. C.; Avouris, P. Thin Film Nanotube Transistors Based on Self-Assembled, Aligned, Semiconducting Carbon Nanotube Arrays. *ACS Nano* **2008**, *2*, 2445–2452.

(17) Joo, Y.; Brady, G. J.; Arnold, M. S.; Gopalan, P. Dose-Controlled, Floating Evaporative Self-assembly and Alignment of Semiconducting Carbon Nanotubes from Organic Solvents. *Langmuir* **2014**, *30*, 3460–3466.

(18) Brady, G. J.; Way, A. J.; Safron, N. S.; Evensen, H. T.; Gopalan, P.; Arnold, M. S. Quasi-ballistic carbon nanotube array transistors with current density exceeding Si and GaAs. *Sci. Adv.* **2016**, *2*, e1601240.

(19) Li, H.; Hain, T. C.; Muzha, A.; Schöppler, F.; Hertel, T. Dynamical Contact Line Pinning and Zipping during Carbon Nanotube Coffee Stain Formation. *ACS Nano* **2014**, *8*, 6417–6424.

(20) Shastry, T. A.; Seo, J.-W. T.; Lopez, J. J.; Arnold, H. N.; Kelter, J. Z.; Sangwan, V. K.; Lauhon, L. J.; Marks, T. J.; Hersam, M. C. Large-Area, Electronically Monodisperse, Aligned Single-Walled Carbon Nanotube Thin Films Fabricated by Evaporation-Driven Self-Assembly. *Small* **2013**, *9*, 45–51.

(21) Zhang, S.-Y.; Liu, J.-W.; Zhang, C.-L.; Yu, S.-H. Co-assembled thin films of Ag nanowires and functional nanoparticles at the liquid–liquid interface by shaking. *Nanoscale* **2013***, 5*, 4223–4229.

(22) Kim, K.; Han, H. S.; Choi, I.; Lee, C.; Hong, S.; Suh, S.-H.; Lee, L. P.; Kang, T. Interfacial liquid-state surface-enhanced Raman spectroscopy. *Nat. Commun.* **2013**, *4*, 2182.

(23) Biswas, S.; Drzal, L. T. A Novel Approach to Create a Highly Ordered Monolayer Film of Graphene Nanosheets at the Liquid−Liquid Interface. *Nano Lett.* **2009**, *9*, 167–172.

(24) Matsui, J.; Yamamoto, K.; Inokuma, N.; Orikasa, H.; Kyotani, T.; Miyashita, T. Fabrication of densely packed multi-walled carbon nanotube ultrathin films using a liquid–liquid interface. *J. Mater. Chem.* **2007**, *17*, 3806–3811.

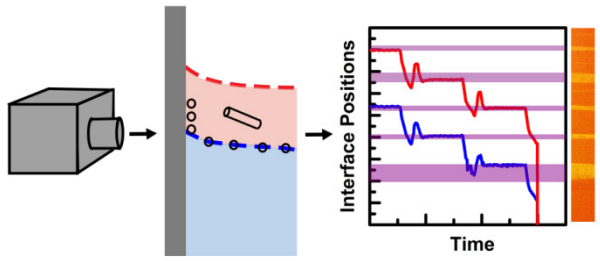


**TOC Figure**